PNAS RESEARCH ARTICLE | DEVELOPMENTAL BIOLOGY

Fin ray branching is defined by TRAP$^+$ osteolytic tubules in zebrafish

João Cardeira-da-Silva[a,b,c,1,2], Anabela Bensimon-Brito[a,b,d,2], Marco Tarasco[a,c], Ana S. Brandão[e], Joana T. Rosa[c,4], Jorge Borbinha[e], Paulo J. Almeida[f], António Jacinto[e], M. Leonor Cancela[c,g], Paulo J. Gavaia[c,g,3], Didier Y. R. Stainier[a,b,3], and Vincent Laizé[c,1,3]

Edited by Neil Shubin, The University of Chicago, Chicago, IL; received May 28, 2022; accepted October 6, 2022

The shaping of bone structures relies on various cell types and signaling pathways. Here, we use the zebrafish bifurcating fin rays during regeneration to investigate bone patterning. We found that the regenerating fin rays form via two mineralization fronts that undergo an osteoblast-dependent fusion/stitching until the branchpoint, and that bifurcation is not simply the splitting of one unit into two. We identified tartrate-resistant acid phosphatase-positive osteolytic tubular structures at the branchpoints, hereafter named osteolytic tubules (OLTs). Chemical inhibition of their bone-resorbing activity strongly impairs ray bifurcation, indicating that OLTs counteract the stitching process. Furthermore, by testing different osteoactive compounds, we show that the position of the branchpoint depends on the balance between bone mineralization and resorption activities. Overall, these findings provide a unique perspective on fin ray formation and bifurcation, and reveal a key role for OLTs in defining the proximo-distal position of the branchpoint.

osteoclasts | bone patterning | bone resorption | bifurcation | fin regeneration

The formation of skeletal structures, such as the limbs or the vertebral column, entails precise patterning processes orchestrated through the activity of multiple cells and signaling pathways (1). Bone formation and homeostasis depend on the synchronized activity of bone-forming (osteoblasts) and -resorbing (osteoclasts) cells (2). Understanding how these cells contribute to the shaping of bones is particularly relevant in the context of bone disease and injury (1).

Although mammals have a limited capacity to regenerate skeletal tissues, except for the digit tips (3), nonmammalian vertebrates, such as zebrafish (*Danio rerio*), are able to regenerate multiple organs and appendages very efficiently (4). In this regard, zebrafish is an established model to study caudal fin regeneration, during which multiple tissues, including bone, are fully restored to their original size and shape (4–7). The process of fin regeneration involves the formation of a blastema, a pool of dedifferentiated cells that form the new tissues, distal to each ray (6, 8). The fin bones, or rays (lepidotrichia), are composed of a mineralized collagenous matrix secreted by osteoblasts and are formed by dermal ossification without a cartilaginous template (9–11). Fin rays are composed of repetitive segments in the proximo-distal axis and by two hemirays (one left and one right) in the transverse plane. Apart from the outermost ones, all rays are bifurcated at different proximo-distal positions, according to the shape of the fin and ray length, i.e., shorter rays branching more proximally and longer rays more distally (12). The proximo-distal positioning of the bifurcations along the rays is critical for the overall fin architecture, as recently highlighted by studies of *collagen9ac1c* zebrafish mutants which display impaired bifurcation associated with fin misshaping (13).

Ray bifurcation is considered as the splitting of a single mineralizing ray into two daughter rays forming a branched structure. This process depends on various signals including those from the adjacent interray tissue (14, 15). Importantly, among the signaling pathways controling bone patterning, such as during limb development (16, 17), Sonic hedgehog (Shh) has been described as a key factor controling ray bifurcation during fin regeneration (18, 19, 20). However, repetitive amputations (21), macrophage activity (22), the organization of actinotrichia (i.e., fibrils located at the tip of each bony ray) (13), and hydrodynamics (23) are able to alter the proximo-distal positioning of ray branchpoints through apparently Shh-independent mechanisms. Thus, the formation and shaping of bifurcated bony structures, and how different cell types contribute to these processes, are still unknown.

Here, we used chemical and genetic tools, together with live-imaging approaches, to investigate how caudal fin rays mineralize and are shaped during regeneration. We show that fin rays mineralize in two lateral fronts that undergo an osteoblast-dependent fusion (stitching) in the center. This stitching process is counteracted by the activity of

Significance

Skeletal function is inherently linked to the correct shaping of the bones. However, how different cells regulate bone shaping remains unclear. The zebrafish fins are particularly suitable to study bone shaping, as bone rays undergo a simple bifurcation process, easily tracked in vivo. Here, we show that the bifurcation of a bone element relies on stitching and antistitching events, rather than on the splitting of a single unit. This report describes tartrate-resistant acid phosphatase-positive (TRAP$^+$) osteolytic tubules and their role in bone bifurcation. Our study provides valuable insights into how cells coordinate to shape bones, thereby contributing to our understanding of bone degenerative and dysmorphic diseases and the identification of new therapeutic strategies.

Author contributions: J.C.-d.-S., A.B.-B., P.J.G., D.Y.R.S., and V.L. designed research; J.C.-d.-S., A.B.-B., M.T., A.S.B., J.T.R., J.B., and P.J.A. performed research; A.J., M.L.C., P.J.G., D.Y.R.S., and V.L. contributed new reagents/analytic tools; J.C.-d.-S. and A.B.-B. analyzed data; M.T., A.S.B., J.T.R., J.B., P.J.A., A.J., M.L.C., P.J.G., D.Y.R.S., and V.L. reviewed and edited the paper; and J.C.-d.-S. and A.B.-B. wrote the paper.

The authors declare no competing interests.

This article is a PNAS Direct Submission.

[1]To whom correspondence may be addressed. Email: joao.cardeira-da-silva@mpi-bn.mpg.de or vlaize@ualg.pt.

[2]J.C.-d.-S. and A.B.-B. contributed equally to this work.

[3]P.J.G., D.Y.R.S., and V.L. contributed equally to this work.

[4]Present address: S^{2}AQUA – Sustainable and Smart Aquaculture Collaborative Laboratory, 8700-194 Olhão, Portugal.

This article contains supporting information online at https://www.pnas.org/lookup/suppl/doi:10.1073/pnas.2209231119/-/DCSupplemental.

Published November 23, 2022.

tartrate-resistant acid phosphatase-positive (TRAP$^+$) osteolytic tubules (OLTs), which define the proximo-distal positioning of the branchpoints through localized osteolytic activity. Overall, we i) provide a detailed analysis of how bony rays are formed and bifurcate, ii) identify OLTs as critical in defining branchpoint positioning, and iii) propose this model to study the (im)balance between bone mineralizing and resorbing activites.

Results

Rays form via Two Mineralizing Fronts that Undergo Gradual Stitching. To understand the morphogenetic processes underlying fin ray formation and bifurcation, we tracked the mineralization of individual rays over time in the adult zebrafish caudal fin postamputation. To ensure consistency, we define "bifurcation" as the process of splitting the mineralized ray, and "bifurcating ray" as a structure characterized by two distinguishable daughter rays separated at a branchpoint (*SI Appendix*, Fig. S1). We found that the onset of bifurcation is variable among individuals, taking place between 3 and 6 days postamputation (dpa; *SI Appendix*, Fig. S2). Therefore, in the present study, we distinguish the "prebifurcation" and "bifurcation" stages irrespective of the postamputation time point. We observed that, during the bifurcation phase, the branchpoints are positioned at more proximal sites (i.e., closer to the amputation plane) in early stages, but gradually distalize over time (i.e., move further away from the amputation plane; Fig. 1 *A*, A' and *B*). These findings indicate that the bony rays form through two mineralizing fronts that undergo a proximal-

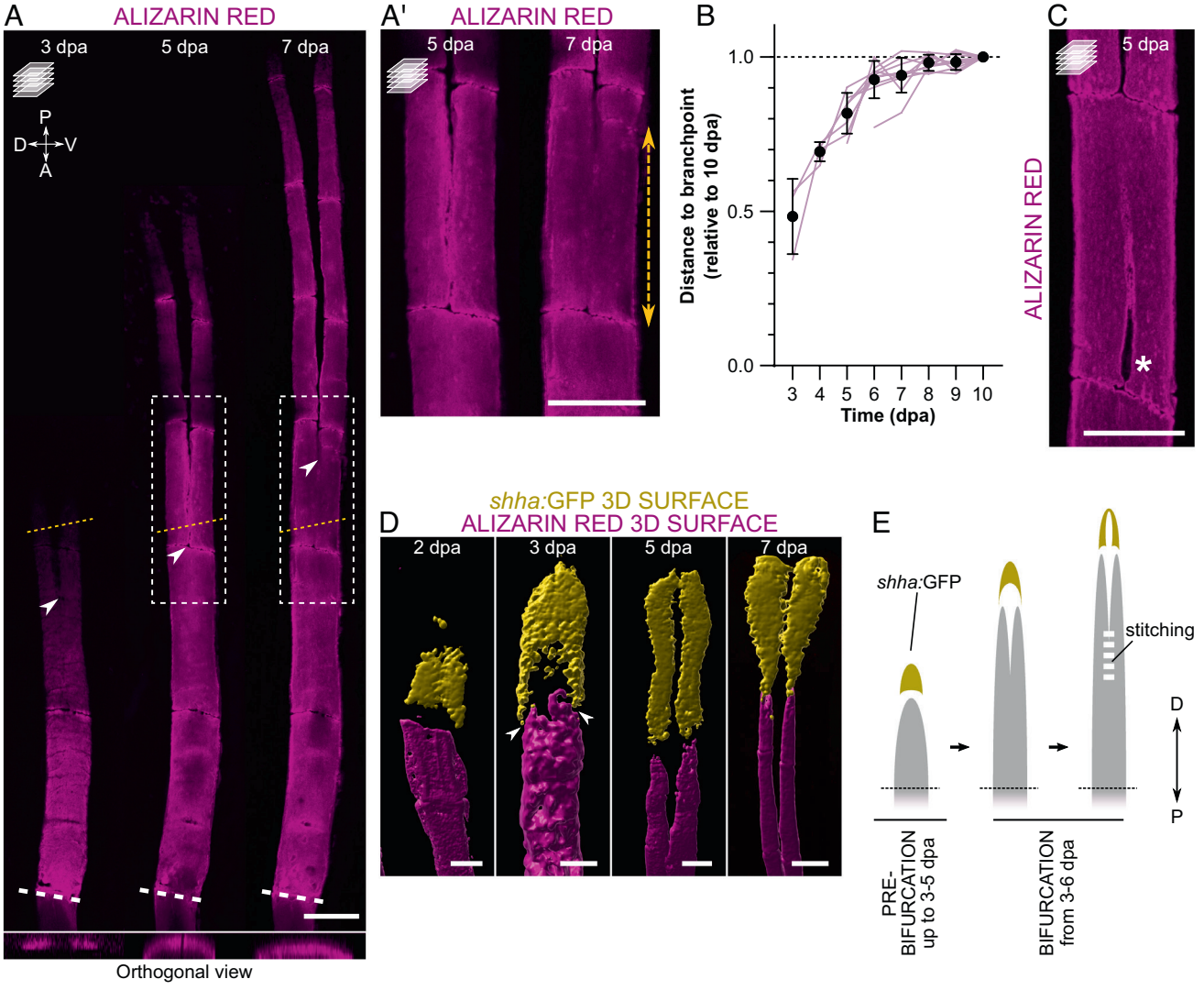

Fig. 1. During bifurcation, fin rays form via two mineralizing fronts that undergo gradual stitching. (*A*, *A*′) Confocal images of representative alizarin red-stained zebrafish, showing the regenerative progression of the same single fin ray and the dynamic position of the branchpoint (arrowheads) over time. Yellow dotted lines indicate the planes of the orthogonal views shown in the *Bottom*; boxes represent the areas magnified in *A*′. Double arrow shows the extension of mineral stitching from 5 to 7 dpa. (*B*) Individual quantitative analysis of the distance from the amputation plane to the branchpoint of dorsal ray #3 at different time points relative to 10 dpa (tracking of individual rays in the same animals from the onset of bifurcation). $N = 3$ for 3 dpa, 4 for 4 dpa, 7 for 5 dpa and 10 for the remaining time points. One-way ANOVA with Geisser–Greenhouse correction ($P < 0.0001$) and Tukey post hoc tests for multiple comparisons (details of statistics for multiple comparisons can be found in *SI Appendix*, Table S1). The graph shows the mean ± SD and values of individual rays (magenta lines). (*C*) Confocal image of a representative bifurcating ray displaying an unstitched portion (asterisk) below the branchpoint. (*D*) 3D surface renderings of representative regenerating rays at different time points, showing the segregation of *shha:*GFP$^+$ domains close to the forming bone (arrowheads) even before the onset of bifurcation, while remaining connected distally. See also *SI Appendix*, Fig. S3. (*E*) Model of ray regeneration divided into the prebifurcation and bifurcation phases, highlighting the timing variability of the different events between specimens, and showing the process of stitching of the two mineralizing fronts. White dashed lines in *A* indicate the amputation plane; the amputation planes in *A*′, *C*, and *D* are not included in the pictures. P, proximal; D, distal. All confocal images are maximum intensity projections. (Scale bars: 100 μm.)

to-distal fusion, a process herein termed "stitching". The stitching of bifurcating rays is clear until at least 7 dpa, when it gradually slows down and the branchpoint position stabilizes at around 9–10 dpa (Fig. 1*B* and *SI Appendix*, Table S1). Moreover, we frequently observed gaps in the mineralized rays proximal to the branchpoint, possibly corresponding to imperfections that occur during the stitching process (Fig. 1*C*).

We then analyzed *sonic hedgehog a* (*shha*) expression with single-cell resolution imaging and observed that, prior to the formation of the two mineralizing fronts, *shha*:GFP$^+$ cells are organized in a single cluster forming a cap-like shape (Fig. 1*D* and *SI Appendix*, Fig. S3). Interestingly, we observed that the proximolateral extensions of this structure were on top of the two mineralizing fronts. These data suggest that the mechanisms of ray segregation are active before the two mineralizing fronts are visible, and that regenerating rays have a predisposition to bifurcate. With the progression of the regenerative and bifurcation processes, *shha*-expressing cell domains become further extended toward the amputation plane while remaining as a single domain. Complete separation of the two *shha*:GFP$^+$ domains occurs at around 7 dpa (Fig. 1*D* and *SI Appendix*, Fig. S3), when the stitching process slows down toward its conclusion, and two daughter rays are clearly observed.

Overall, we show that, at least during part of the outgrowth, bony rays regenerate via two mineralizing fronts that progress in tandem and undergo a proximal-to-distal stitching up to the final position of the branchpoint (Fig. 1*E*).

Osteoblasts Mediate the Stitching of the Two Mineralizing Fronts. To better understand the mechanisms and biological processes taking place during ray regeneration and bifurcation, we performed RNA-Seq on regenerates at 1 dpa (i.e., prior to new bone mineralization) (12) and 3 dpa (i.e., at, or shortly preceding, the appearance of the two mineralizing fronts and the cap-like *shha* single domain; *SI Appendix*, Fig. S4*A*). As expected, while various early blastema marker genes (e.g., *msx2b*, *fgf20a*, *wnt5a*) were down-regulated, several osteogenesis- and morphogenesis-related genes (e.g., *sp7*, *col10a1a*, *bglap*, *alpl*, *hoxb13a*, *hoxd13a*) were up-regulated at 3 dpa in comparison with 1 dpa (*SI Appendix*, Fig. S4*B*). Moreover, gene ontology terms related to extracellular matrix (ECM) were shown to be enriched at 3 dpa (*SI Appendix*, Fig. S4*C*). These ECM proteins include collagens and other structural components, as well as ECM regulators (*SI Appendix*, Fig. S4*D*). Importantly, osteoblast-related genes, such as *bone gla protein* (*bglap*) and *sp7 transcription factor* (*sp7*), and genes encoding bone matrix components, namely *collagen type I* (e.g., *col1a1a*, *col1a1b*, *col1a2*) and *collagen type X* (e.g., *col10a1a*), were up-regulated at 3 dpa (*SI Appendix*, Fig. S4*E*).

With these data, we hypothesized that osteoblasts, known to drive the formation of new bone in regenerating fin rays (24, 25), are also involved in bone patterning and mediate the stitching process. Accordingly, using *bglap:GFP* reporter zebrafish, we observed osteoblasts at the stitching sites (Fig. 2*A*). To determine the role of osteoblasts during the stitching process, we performed cell-specific ablation using the *sp7*:mCherry-NTR line (25). Zebrafish were exposed to metronidazole (Mtz) for 24 h, starting at 3 dpa, to maximize the depletion of osteoblasts (Fig. 2*B*). Fluorescence intensity analysis confirmed the decrease in the *sp7*:mCherry-NTR signal at the end of the Mtz treatment and a recovery at later stages (*SI Appendix*, Fig. S5 *A* and *B*), thereby validating the osteoblast ablation protocol, as previously described (25). At 7 dpa, wild-type Mtz-treated zebrafish did not show

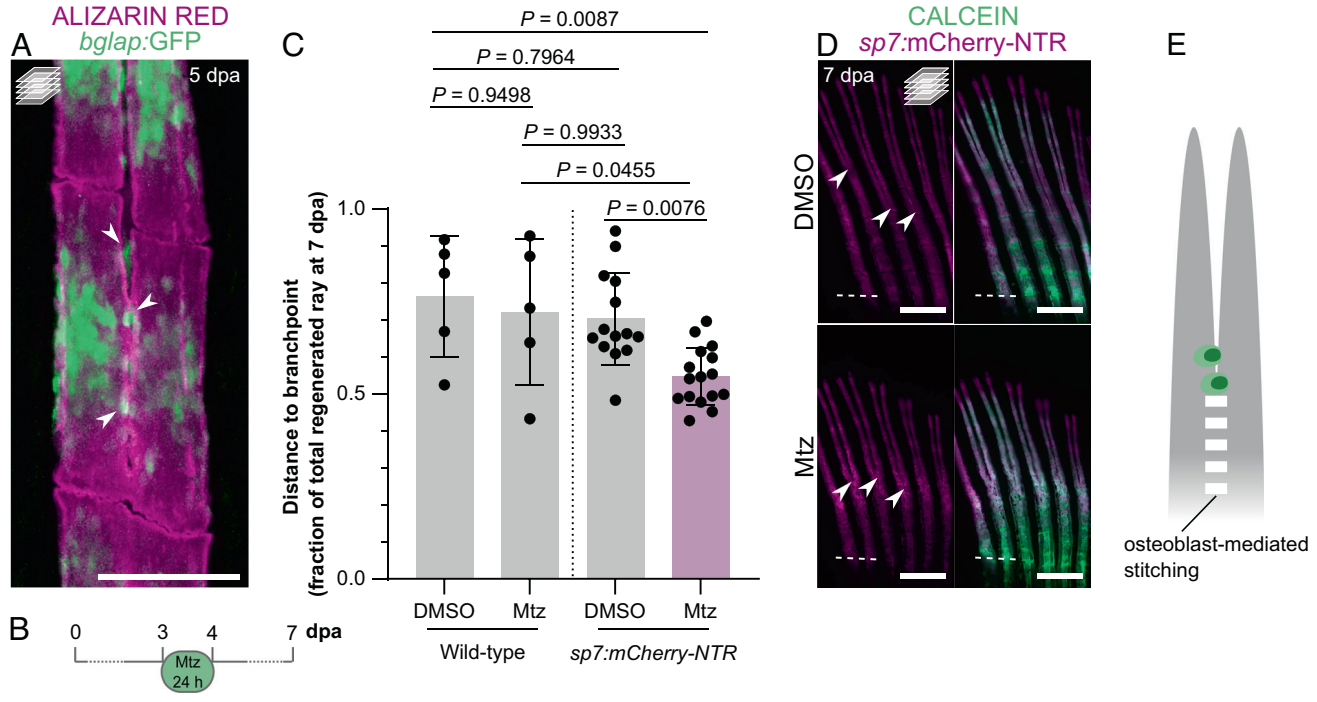

Fig. 2. Osteoblast ablation induces branchpoints closer to the amputation plane. (*A*) Confocal image of a representative bifurcating alizarin red-stained ray, showing mature osteoblasts at the stitching zone (arrowheads). (*B–D*) Ablation of *sp7*:mCherry-NTR$^+$ osteoblasts during early bifurcation. (*B*) Ablation protocol. (*C*) Quantification of the relative distance from the amputation plane to the branchpoint at 7 dpa following Mtz treatment in wild-type and *sp7:mCherry-NTR* zebrafish, showing a clear shift of the branchpoint closer to the amputation plane after osteoblast ablation. The dots in the graph represent individual zebrafish, and the bars represent the mean ± SD. One-way ANOVA ($P = 0.0013$) and Tukey's post hoc test. (*D*) Confocal images of representative regenerates of Mtz-treated zebrafish compared with control/DMSO-treated individuals, showing branchpoints closer to the amputation plane (arrowheads). (*E*) Model placing osteoblasts as key players in the stitching process. Dashed white lines in *D* mark the amputation planes. All confocal images are maximum intensity projections. (Scale bars: 100 µm in *A*; 500 µm in *D*.)

significantly different branchpoint positions when compared with DMSO-treated ones (Fig. 2*C* and *SI Appendix*, Fig. S5*C*). However, *sp7*:mCherry-NTR Mtz-treated zebrafish displayed branchpoints closer to the amputation plane when compared with controls (Fig. 2 *C* and *D*). To check whether the effect on branchpoint positioning was secondary to the reduction of ray length due to pan-osteoblast ablation (*SI Appendix*, Fig. S5*D*), we compared these individuals with untreated wild-type zebrafish exhibiting rays of comparable length (6 dpa; *SI Appendix*, Fig. S5*D*). Also in this case, the Mtz-treated transgenic zebrafish presented rays with branchpoints closer to the amputation plane (*SI Appendix*, Fig. S5*E*). Therefore, the presence of osteoblasts at the stitching points and the impaired stitching of the two mineralizing fronts of each ray upon their ablation highlight the potential importance of osteoblasts in mediating this process (Fig. 2*E*).

OLTs are Central to Ray Bifurcation. Osteoblasts and osteoclasts display opposing, yet cross-balanced, activities in numerous settings of bone formation and homeostasis (1). In fact, our RNA-Seq data show that together with osteoblast-, bone formation- and bone matrix-related genes, regulators of osteoclastogenesis, such as *tumor necrosis factor receptor superfamily, member 11a, NFKB activator* (*tnfrsf11a*) and *colony stimulating factor 1 receptor b* (*csf1rb*), were also up-regulated at 3 dpa (*SI Appendix*, Fig. S4*E*). Therefore, we analyzed the osteoclast dynamics during the bifurcation process. By using the *ctsk:DsRed* line, which labels active mature osteoclasts (26), we found that *cstk:*DsRed^{+} cells display distinct morphologies and localizations at the different phases of ray bifurcation (Fig. 3). In the prebifurcation phase, during the stitching process, osteoclasts are round, exhibit cytoplasmic extensions, and accumulate mostly inside the regenerating rays (i.e., between the two hemirays; Fig. 3 *A* and *B*). In contrast, during the bifurcation phase, osteoclasts form elongated structures that line up along the branching ray surface and border the outer limits of the regenerating bone (Fig. 3 *C* and *D*). To test whether these elongated osteoclast structures display bone resorbing activity, we stained the regenerating fins at the bifurcation phase for the activity of tartrate-resistant acid phosphatase (TRAP), an

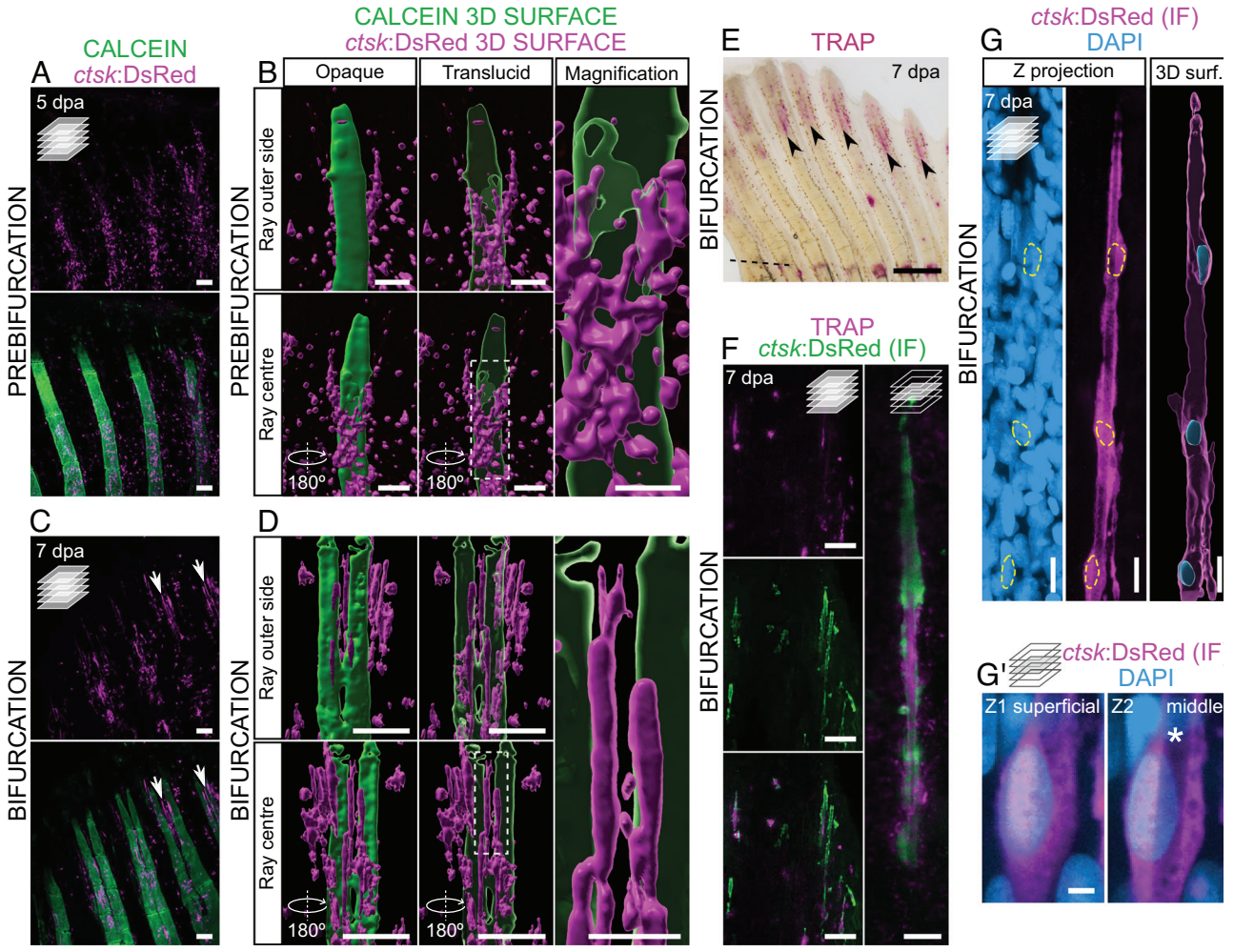

Fig. 3. TRAP-secreting osteolytic tubules align with the bone surface at ray splitting regions during bifurcation. (*A–D*) Confocal images (*A and C*) and 3D surface renderings (*B and D*) of *ctsk*:DsRed expression in representative calcein-stained regenerating fins at the prebifurcation (*A and B*) and bifurcation (*C and D*) stages. 3D surface renderings are shown in two different perspectives and the mineralized surface is shown as opaque and translucid; 3D reconstructions represent one hemiray and the center of the ray, but not the entire ray. Boxes represent the areas magnified on the *Right*. Arrows point to osteolytic tubules. (*E*) Stereomicroscope image showing TRAP activity at the splitting region (arrowheads) of representative bifurcating rays. (*F*) Confocal images of elongated osteoclasts at the splitting region, following immunofluorescence (IF) staining for DsRed and stained for TRAP activity. (*G*) Confocal images and 3D surface rendering of a single representative osteolytic tubule following IF for DsRed, highlighting DAPI-stained nuclei (outlined by yellow dashed lines). See also Movie S1. (*G′*) Single osteolytic tubule nucleus at two different Z planes, showing a preserved nonfluorescent lumen (asterisk) at the nuclear sites. See also Movie S2. Dashed line in *E* marks the amputation plane. Single confocal planes in *F* and *G′ Right*; all remaining confocal images are maximum intensity projections. (Scale bars: 100 µm in *A–D* (lower magnifications in *B* and *D*); 30 µm in higher magnifications in *B* and *D*; 500 µm in *E*; 50 and 10 µm in *F Left* and *Right*, respectively; 10 µm in *G*; 2 µm in *G′*.)

osteoclast-specific secreted enzyme involved in bone resorption (27). We observed that TRAP signal strongly accumulates at the branching sites (Fig. 3*E*) and colocalizes with the *ctsk:*DsRed^{+} cells (Fig. 3*F*), indicating that these cells display bone-resorbing activity. We also observed that these *ctsk:*DsRed^{+} elongated structures exhibit a nonfluorescent lumen and, therefore, we name them osteolytic tubules (OLTs). Interestingly, TRAP activity signal strongly accumulates within the lumen of OLTs (Fig. 3*F*). We also determined the distribution of nuclei within each tubule and found that OLTs are composed of a few nuclei located at bulging sites, with long nuclei-free projections (Fig. 3*G* and Movie S1). However, it remains unclear whether these tubules are composed of mono- or multinucleated cells. Moreover, we show that the OLT nuclei are located at peripheral positions, away from the nonfluorescent lumen (Fig. 3*G*′and Movie S2).

To determine whether OLTs are specific to regeneration, we analyzed uninjured fins and observed that they display little *ctsk:*DsRed signal, with only a few OLTs at the distal tips of the permanently growing fin rays (Fig. 4*A*). This observation indicates that OLTs are not specific to the regenerative process and that they are also associated with fin rays in different developmental contexts. In fact, OLTs are also abundant in developing fins (Fig. 4 *B* and *C*). To further characterize the OLTs, we assessed the expression of different reporter transgenes in developing and regenerating fins. Because osteoclasts and macrophages share a common lineage, we imaged OLTs in the *mpeg1.1:YFP* background and observed that they form distinct populations. However, they seem to physically interact (Fig. 4*D*), suggesting that the immune system may play a role in regulating the OLTs and/or vice-versa. Using the *fli1:GFP* reporter line, we observed that OLTs lie in close proximity to blood vessels, during both development and regeneration (Fig. 4*E*), also suggesting a relationship between OLTs and the vasculature. Intriguingly, we observed that OLTs express the *lyve1b:GFP* lymphatic endothelial reporter (Fig. 4*F*).

Altogether, these data show the presence of OLTs during bone development and regeneration, particularly in association with

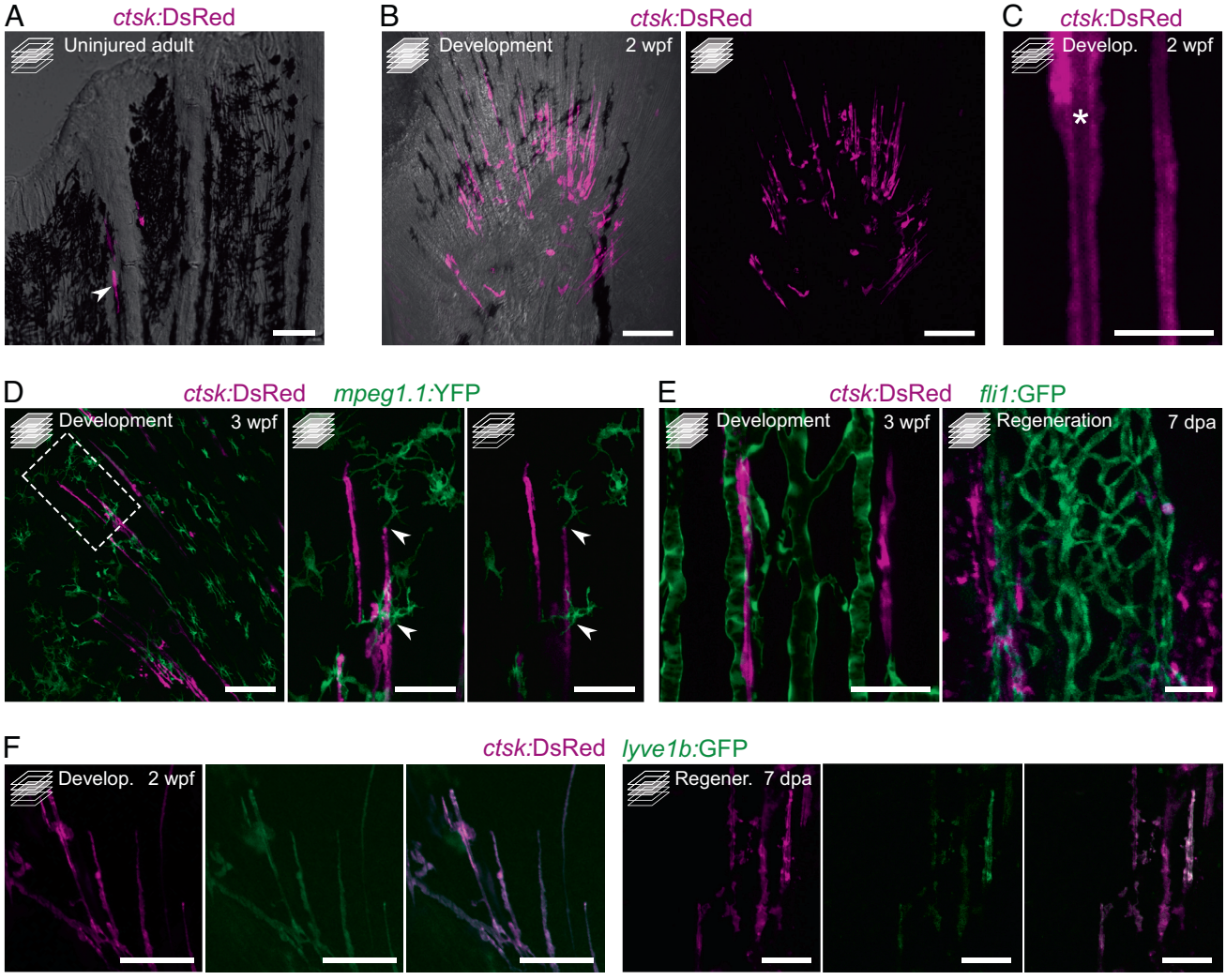

Fig. 4. Osteolytic tubules are present in the developing fin, display a tubular morphology, interact with macrophages, align with blood vessels, and are positive for *lyve1b*:GFP. (*A*) Confocal image of representative adult uninjured caudal fin displaying *ctsk*:DsRed^{+} osteoclasts at the growing edges of rays. (*B and C*) Confocal images of representative developing caudal fin showing elongated osteoclast structures aligned with fin rays (*B*) displaying a tubular morphology with a nonfluorescent lumen (asterisk) (*C*). (*D*) Confocal images of representative developing pectoral fin, showing direct interaction between macrophages (green) and tubular osteoclasts. Box represents the areas magnified on the *Right*. (*E*) Confocal images showing tubular osteoclasts aligning with blood vessels (green) during caudal fin development and regeneration (*Left* and *Right*, respectively). (*F*) Confocal images showing that tubular osteoclasts are positive for *lyve1b*:GFP, during caudal fin development and regeneration (sets of images on the *Left* and *Right*, respectively). Maximum intensity projections in *B* and *D* (lower magnification and higher magnification on the *Left*) and *E*. Single confocal planes in *A*, *C*, and *D* (higher magnification on the *Right*) and *F*. (Scale bars: 50 μm in *A* and *D* (higher magnifications), *E* and *F*; 100 μm in *B* and *D* (lower magnification); 10 μm in *C*.)

ray branchpoints, possibly interacting with the immune and vascular systems.

Bone Resorbing Activity of OLTs is Required for Bifurcation. Given the presence of OLTs at the branching sites, we investigated whether they are required during the ray bifurcation process. A single dose of salmon calcitonin, a strong antiresorbing agent (28), also active in zebrafish (29, 30), was injected intraperitoneally simultaneously with the amputation procedure, and ray regeneration was tracked overtime (Fig. 5*A*). We observed a strong impairment of ray bifurcation in calcitonin-injected zebrafish, compared with DMSO-injected control individuals (Fig. 5*B*), as shown by branchpoints further away from the amputation plane (Fig. 5*C*) and a reduction in the number of rays displaying signs of bifurcation at 7 dpa (*SI Appendix*, Fig. S6*A*), in all concentrations tested. At 14 dpa, when the regenerative process is close to conclusion, branchpoints far away from the amputation plane were still markedly evident (*SI Appendix*, Fig. S6*B*), with some zebrafish presenting no bifurcated rays at all. Because the highest calcitonin concentration (50 µg/g) caused high phenotypic variability and heterogeneity in mineralization density (i.e., variable alizarin red staining intensity within individual fins; *SI Appendix*, Fig. S6*C*), and the lowest concentration (0.5 µg/g) was enough to induce a bifurcation phenotype, subsequent analyses were carried out at 0.5 µg/g to avoid nonspecific effects of the drug. To test whether the calcitonin treatment was indeed inhibiting bone resorption

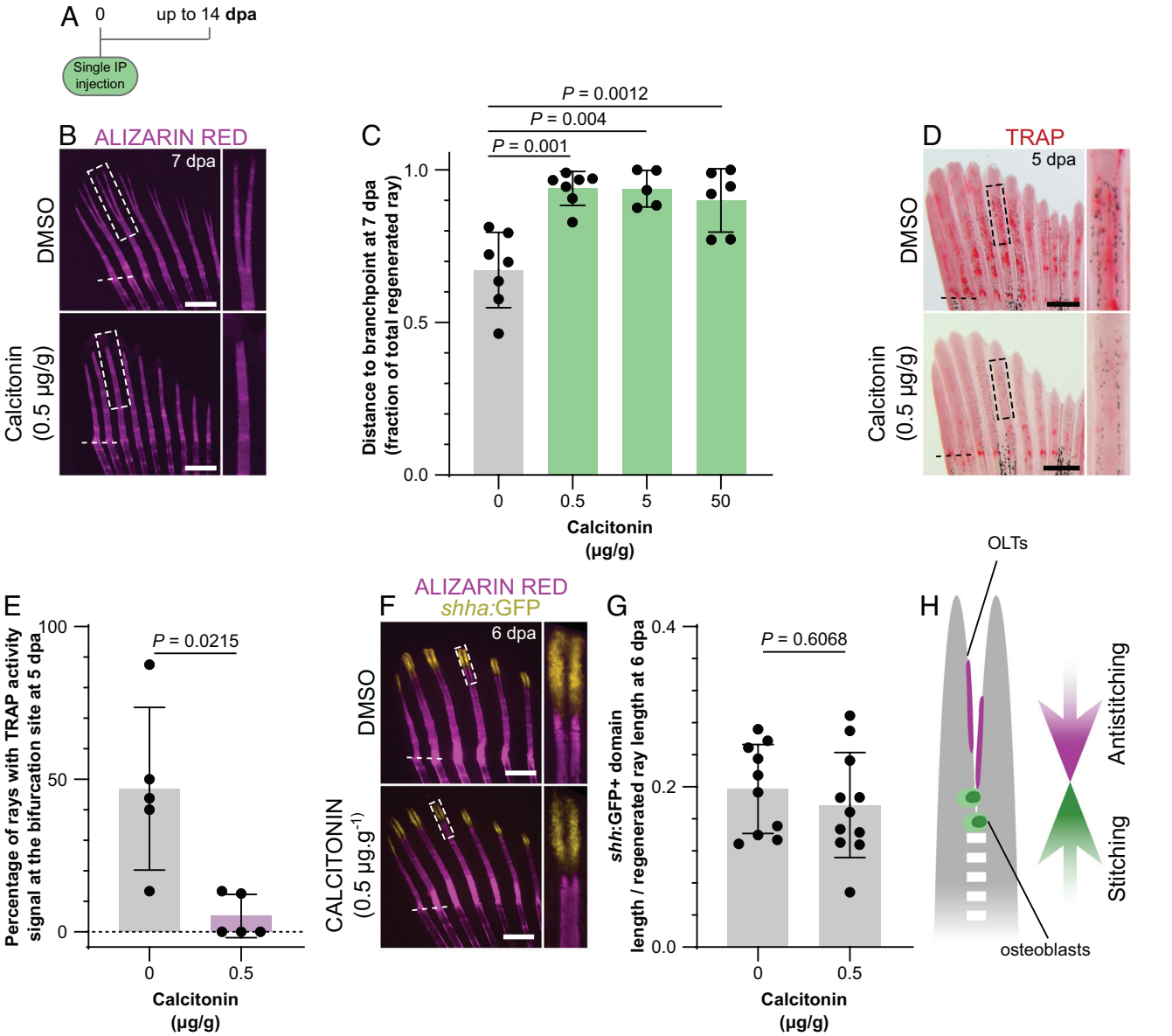

Fig. 5. Inhibition of osteoclast activity impairs ray bifurcation. (*A*) Calcitonin treatment experimental protocol. (*B and C*) Stereomicroscope images of representative mineralized rays (B) and quantification (*C*) of the relative distance from the amputation plane to the branchpoint at 7 dpa, showing impaired bifurcation upon calcitonin treatment. Boxes in *B* represent the areas magnified on the *Right*. (*D and E*) Stereomicroscope images of representative TRAP-stained fins (*D*) and quantification of the percentage of rays displaying TRAP signal at the bifurcation site (*E*) at 5 dpa, showing reduced osteoclast activity upon calcitonin treatment. Boxes in *D* represent the areas magnified on the *Right*. (*F and G*) Confocal images of representative bifurcating rays showing segregation of the *shha:*GFP^{+} domains (*F*) and quantification of their extension (*G*), confirming that calcitonin effects are Shh-independent. Boxes in *F* represent the areas magnified on the *Right*. (*H*) Model highlighting the balanced stitching and antistitching activities of osteoblasts and OLTs to define the branchpoint position. The dots in the graphs represent individual zebrafish; all graphs show the mean ± SD. One-way ANOVA ($P = 0.0057$) and Tukey's post hoc test in *C*; unpaired, two-tailed Student's *t* test with Welch's correction in *E*; unpaired, two-tailed Student's *t* tests in *F*. (Scale bars: 500 µm.)

activity, we analyzed TRAP accumulation at 5 dpa and observed a significant reduction in the treated zebrafish (Fig. 5*D*). The number of rays displaying TRAP activity at the bifurcation site was also drastically reduced in calcitonin-treated zebrafish (Fig. 5*E*), confirming the effectiveness of this drug in reducing bone resorbing activity. Interestingly, inhibition of bifurcation and branchpoints far away from the amputation plane were not accompanied by an impaired segregation or different lengths of the *shha:*GFP$^+$ domains (Fig. 5 *F* and *G*). These results indicate that, apart from the role of Shh signaling in mobilizing preosteoblasts and inducing ray splitting (19), the positioning of branchpoints is not dependent on Shh signaling but requires additional cellular and molecular players.

Taken together, our data show that the bone resorbing activity of OLTs contributes to ray bifurcation, and we propose that OLTs function to counteract osteoblast-mediated stitching and, thereby, define the positioning of the branchpoints in developing and regenerating rays (Fig. 5*H*).

Branchpoints as Indicators of Bone Mineralization and Resorption. After establishing the cooperative action of osteoblasts and OLTs in defining the positioning of the branchpoints, we evaluated whether the bifurcation process could represent an adequate readout of imbalanced activities of these cell types. For that end, we exposed amputated zebrafish to different drugs with known proresorbing (dexamethasone and prednisolone) (31), promineralogenic (ibandronate) (32) or osteotoxic properties when in excess (retinoic acid) (33). Treatments with the corticosteroids dexamethasone and prednisolone resulted in branchpoints closer to the amputation plane at 5 dpa, when compared with control zebrafish (Fig. 6 *A*–*C*), indicating decreased stitching and/or increased antistitching activity. The highest concentration of prednisolone even induced trifurcations (Fig. 6*A*), suggesting that the bone rays may have more than one simultaneous branchpoint leading to skeletal malformations. In parallel, we tested the effects of retinoic acid, known to disrupt osteoblast boundaries and to block osteoclast differentiation during fin regeneration (34, 35). As observed with calcitonin, treatment with retinoic acid resulted in branchpoints to become further away from the amputation plane than in controls and induced an almost complete blockage of bifurcation, even when observed at 7 dpa (Fig. 6 *D* and *E*), likely by increased stitching and/or decreased antistitching activity. However, this drug also results in deformed and shorter regenerating rays, which may cause a delay in bifurcation. Therefore, we tested ibandronate, a bisphosphonate widely used as antiresorbing drug, which also resulted in branchpoints far away from the amputation plane, when compared with control zebrafish (Fig. 6 *F* and *G*). This result indicates increased stitching and/or decreased antistitching activity of ibandronate.

Altogether, these data indicate that branchpoint positioning is the result of balanced bone mineralization and resorption. Therefore, this model constitutes a fast readout to assess the properties of several agents during bone formation, considering the osteoblast-mediated stitching and OLT-mediated antistitching activities (Fig. 6*H*).

Discussion

Redefining the Phases of Ray Mineralization in the Regenerating Zebrafish Caudal Fin. Despite extensive investigation of the mechanims regulating bone formation, much remains unknown on how bone size, shape, number, and organization are defined. This process, known as bone patterning, has been widely studied in the vertebrate limb (36). Although the teleost caudal fins have no homology with tetrapod appendages, they share many of the mechanisms activated during limb and digit development, including regulation by common pathways such as Hox and Shh (37–40). Furthermore, the caudal fin regeneration model is a unique platform for live-imaging approaches to study the cellular and molecular events taking place during de novo bone formation in adult animals (7).

So far, most studies have focused on the origins of osteoblasts, their dedifferentiation and redifferentiation, and spatiotemporal organization (24, 25, 41–44), without giving special attention to the mineralization process itself. Here, we focused on understanding how a single ray mineralizes and bifurcates. Shh signaling is required for the ray bifurcation process (18, 19, 20, 45, 46). Recently, *shha*-expressing cells were shown to guide preosteoblasts and position them to form the fin rays during regeneration. Accordingly, the splitting of these domains induces the segregation of two equally discrete populations of preosteoblasts, thus driving ray branching (19). However, as previously suggested, Shh signaling may not be solely responsible for ray bifurcation (21), hence raising the hypothesis that additional morphogenetic/cellular mechanisms are required. Using live-imaging approaches, we identified two mineralization fronts, indicating that the bifurcation process does not simply consist of the separation of one unit into two, but instead it results from the disruption of a fusion/stitching process between two predefined units.

Overall, we propose that ray bifurcation involves several stages. First, the morphogenetic action of molecules like Shh triggers the early division of the mineralizing ray by patterning preosteoblasts in two parallel domains on the flanks of the ray, as described by Armstrong and colleagues (19). Second, the two mineralizing fronts fuse/stitch, through an osteoblast-dependent process. Third, an antistitching activity counteracts the fusion between the two mineralization fronts and defines the positioning of the branchpoint (Fig. 7).

Knowing that bone development and homeostasis result from the balanced activity of osteoblasts (i.e., to form new bone) and osteoclasts (i.e., to resorb bone), we hypothesized that osteoclasts or osteoclast-like cells could be actively mediating the antistitching process. Accordingly, we identified TRAP$^+$ OLTs located at the branching sites, and these cells regulate the proximodistal positioning of the branchpoints (Fig. 7). OLTs display a nonfluorescent lumen which suggests that they may be surrounding other structures, such as actinotrichia. In fact, actinotrichia have recently been sugested to have a role in ray bifurcation and in preventing ray fusion (13). Another hypothesis is that OLTs are perfused with a liquid substance or accumulate osteolytic enzymes, thereby, explaining the observed accumulation of TRAP within the OLTs.

Osteoblasts and osteoclasts are known to communicate through direct interaction or cytokine secretion to regulate cell differentiation, apoptosis, and patterning (2). Therefore, we hypothesize that osteoblasts recruit osteoclast-like cells to the branching sites through the secretion of molecules like M-CSF, RANKL/OPG, as it occurs during bone remodeling (2). Osteoclasts are also known to secrete inhibitors of osteoblast differentiation, such as SEMA4D (47), which would further enhance the antistitching of OLTs.

Overall, we show that, in addition to the central role osteoblasts play in secreting and patterning the bone matrix, osteoclast-like cells are important players in defining the splitting of a single bony ray into two.

The Role of Distinct Osteoclast-Like Cells in Multiple Developmental and Regenerative Contexts. Osteoclasts are myeloid-derived cells (48, 49) responsible for bone resorption

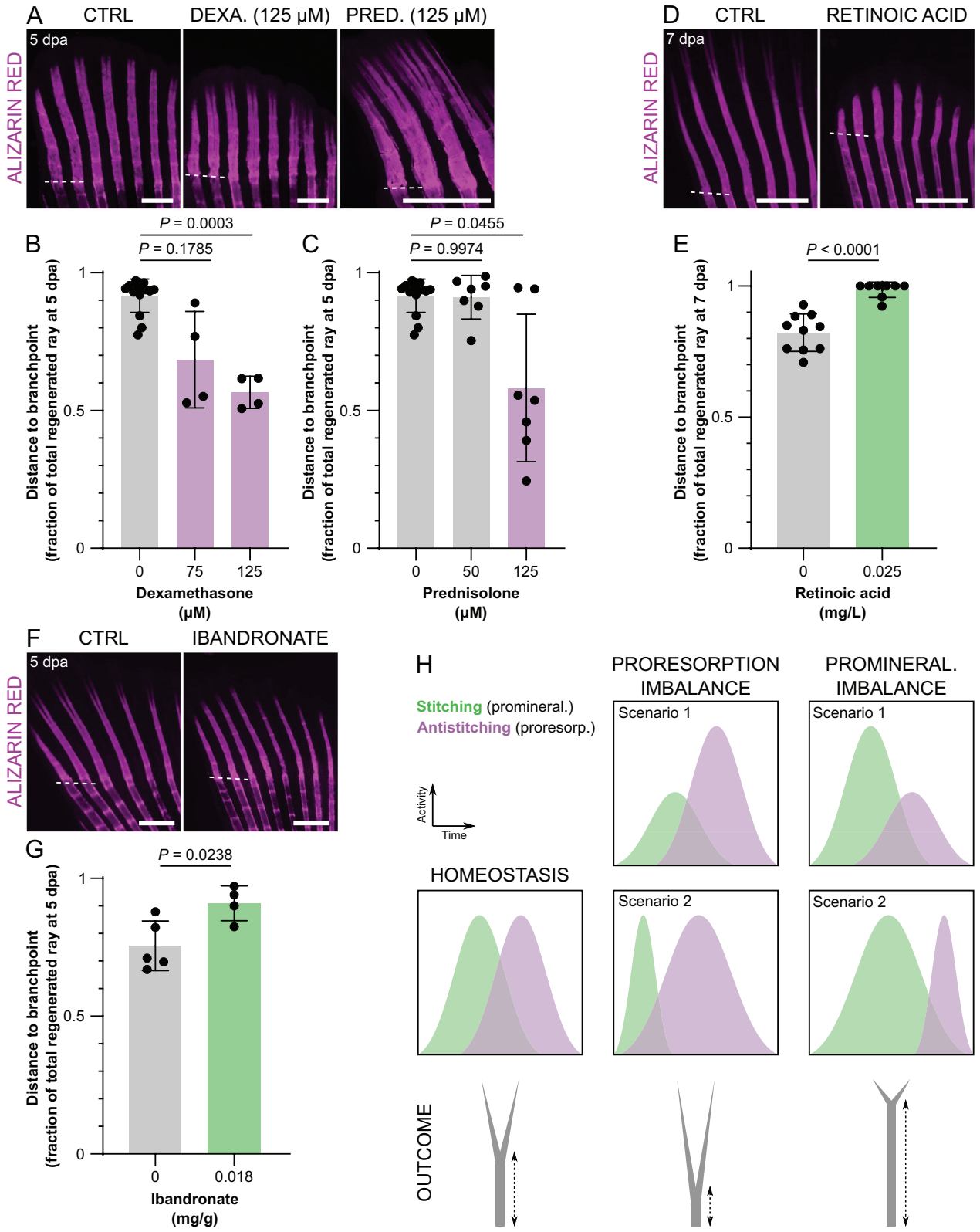

Fig. 6. Branchpoint position, a proxy of ray bifurcation, is a fast readout of proresorption and promineralization imbalance during bone formation. (*A*–*G*) Confocal images (*A, D,* and *F*) and quantification (*B, C, E,* and *G*) of representative mineralizing rays showing branchpoint positioning upon treatment with dexamethasone (*A* and *B*), prednisolone (*A* and *C*), retinoic acid (*D* and *E*), and ibandronate (*F* and *G*). (*H*) Model depicting how the position of the branchpoints represents proresorption and promineralization imbalance. In scenario 1, the imbalance is due to altered intensity of stitching/antistitching activities; in scenario 2, the imbalance is due to altered duration of stitching/antistitching activities. The dots in the graphs represent individual zebrafish; all graphs show the mean ± SD. Welch one-way ANOVA in *B* ($P = 0.0004$) and *C* ($P = 0.0310$) and Dunnett T3 post hoc tests for multiple comparisons; two-tailed Student's *t* test with Welch's correction in *E*; two-tailed Student's *t* test in *G*. (Scale bars: 500 µm.)

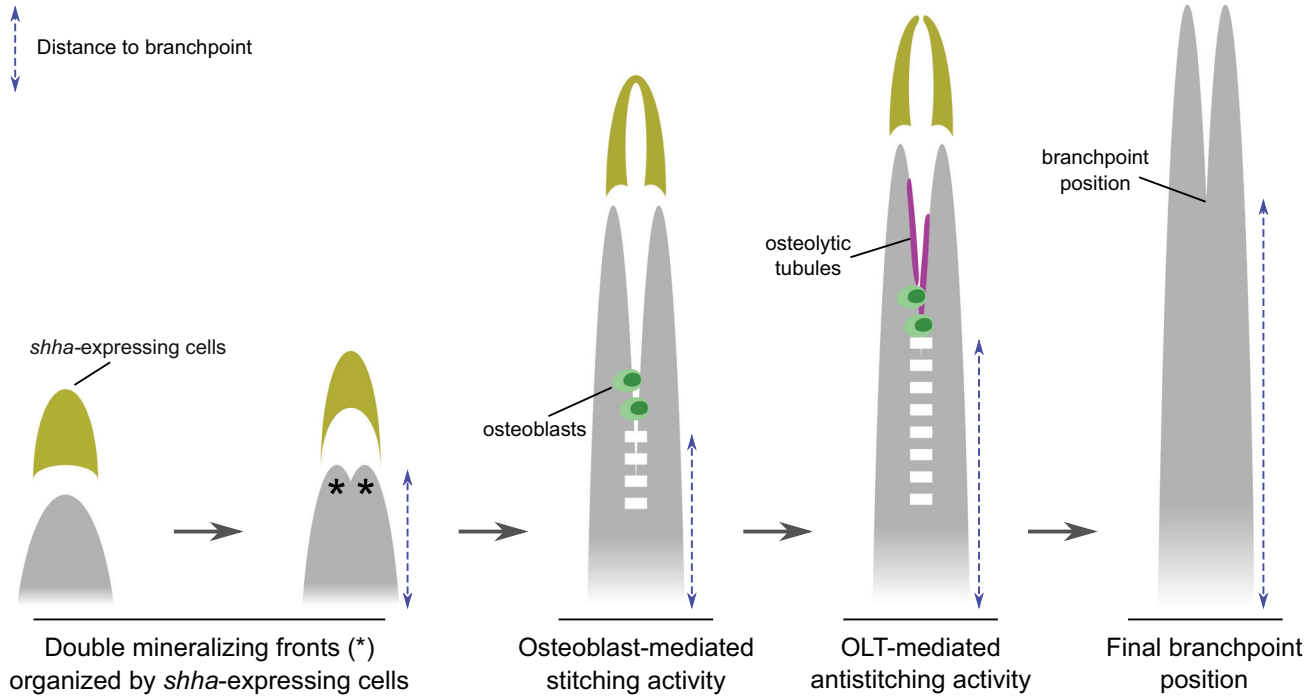

Fig. 7. Proposed model of fin ray bifurcation. The model shows two Shh-guided (yellow) mineralizing fronts (asterisks) that undergo an osteoblast-dependent (green) stitching (dashed white line) to form a ray (gray). This stitching activity is then counteracted by antistitching activity by TRAP$^+$ osteolytic tubules (magenta), thereby defining the branchpoint positioning.

through the acidification of the bone surface and the secretion of proteolytic enzymes (50–53). These enzymes include cathepsin K (Ctsk) (54–57), metalloproteinases (58), and TRAP (59, 60). TRAP is a *bona fide* marker used to assess osteoclast activity in mammals (61, 62) and in teleosts, including zebrafish (27, 35).

Recent studies brought a unique perspective on osteoclasts and TRAP activity, which deviates from their classical role in bone resorption. As other monocytic cells, osteoclasts exhibit high plasticity depending on their environment and have the ability to modulate immune responses, including immunosuppression and inflammation (61). Osteoclasts may also play a non–bone-resorbing role during endochondral ossification, by controlling blood vessel anastomosis (62), or in the development of bone lymphatics, possibly by carving paths for the lymphatic endothelial cells (63). Furthermore, osteoclasts have also been shown to express VEGF-C, a lymphatic growth factor (64), and thus they may directly regulate lymphatic formation within the bone. In contrast, endothelial cells may replace osteoclast function in particular settings and secrete proteolytic enzymes essential for cartilage resorption and directional bone growth (62). Moreover, lymphatic endothelial cells secrete colony-stimulating factor 1 (Csf1) to promote osteoclast formation and regulate bone resorption (63). Noncanonical mechanisms of bone proteolysis, particularly those involving nonclassical osteoclast-like cells and their role in regulating bone formation and shaping, are largely uncharacterized in zebrafish.

TRAP activity has been previously observed in the regenerating fin (34). Yet, in that paper the authors used TRAP to infer on osteoclast activity but no cellular or molecular markers were used to identify the cells secreting this enzyme. Therefore, the precise localization of osteoclast-like cells, their morphology, their spatial-temporal dynamics, and their function during the regenerative process remained unknown. Here, we show that, during the prebifurcation phase, TRAP activity is associated with *ctsk*$^+$ round osteoclast-like cells exhibiting cytoplasmic extensions, located mostly inside the regenerating rays. During the bifurcation phase, we show that TRAP-positive cells (i.e., OLTs), also positive for the *ctsk* reporter$^+$, form tubular structures and align on the bone surface at the branching regions of the regenerating rays. Moreover, we found that OLTs are not specific to regeneration settings, but are also present during fin ray development. Takeyama and colleagues have described distinct populations of osteoclasts in the medaka caudal fin bone fracture healing model (65). In their study, osteoclasts do not form elongated structures and are highly multinucleated. In our model, it remains unclear whether OLTs are composed of tightly aligned mononuclear cells or multinucleated cells. Nevertheless, we show that OLTs contain only a few nuclei, and do not resemble those in the previous study, suggesting that these populations are distinct. We do not, however, exclude the possibility of both populations deriving from a common precursor. Altogether, these observations support a model in which different osteolytic cells/structures are context-specific, with OLTs being required to remodel bone during bifurcation and proximal-to-distal bone growth.

Interestingly, OLTs also express a reporter transgene for *lyve1b*, a widely used marker of lymphatic endothelial cells and fluorescent granular perithelial cells in zebrafish (66, 67) that may also label some macrophages, as reported in mouse (68). Future work will address the exact origin of OLTs and their association with the vascular and/or lymphatic systems. A recent study showed that lymphatics are required for cardiac regeneration in zebrafish (69). The authors described isolated lymphatic sprouts in the injured area that are not connected with the lymphatic network of the uninjured tissue, suggesting that these cell clusters are specifically activated in response to injury. Therefore, it will be interesting to investigate whether a similar process takes place in the regenerating fin and how such process relates with TRAP activity and bone shaping.

Models to Assess Bone Mineralization-to-Resorption Balance. We hypothetize that the exact positioning of the branchpoint depends on a fine-tuned balance between pro- and antistitching activities. Identification of compounds with osteogenic potential (i.e., promineralogenic and/or antiresorbing) can greatly contribute to the

study of bone biology and to the establishment of new therapeutic targets to treat bone disorders or block disease progression.

Owing to the many advantages of using the zebrafish regenerating caudal fin model, [e.g., its suitability for the in vivo assessment of de novo bone formation using live-staining and live-imaging approaches (70)], we and others have described technical strategies for drug screening with focus on bone mineralization (12, 71–73). However, considering that a variety of bone diseases are the result of dysregulated bone resorption, ranging from enhanced bone loss in osteoporosis to increased bone density in osteopetrosis (74), it is important to establish a straightforward model to study bone-resorbing activity and its balance with bone formation. Here, we show that ray branchpoints are established during zebrafish caudal fin regeneration through a direct action of $TRAP^+$ OLTs. We also show that inhibition of bone-resorbing activity is sufficient to shift the branchpoints to a more distal position (Fig. 6), which can be used as a clear readout of resorption-to-mineralization imbalances. Accordingly, several reports have documented multiple factors leading to altered branchpoint positions in the zebrafish regenerating caudal fins rays. A retinoic acid-induced inhibition of bifurcation was previously proposed by White and colleagues (75), an effect that we reproduced and show in detail in the present study. Yet, retinoic acid is a well-known regulator of the proximal–distal identity of appendages and other organs (76) and, therefore, may control ray branching independently of OLT activity. In addition, it raises the question of if and how positional identity mechanisms regulate OLTs into defining the final branchpoint position. Apart from retinoic acid, branchpoints were shown to shift to more distal positions upon inhibition of the Calcineurin pathway (77), known to promote osteoclastogenesis (78). Recently, we showed that an antimineralization/proresorption imbalance induced by benzo[α]pyrene resulted in branchpoints at more proximal positions (79). Ablation of *mpeg1*-positive macrophages, a potential source and/or regulator of the OLTs, resulted in a reduced number of bifurcated rays (22). Interestingly, a recent study proposed that ray branching is modulated by biomechanical forces (23). In fact, bone formation is well known to rely on the mechanosensitive properties of bone-forming cells that, in addition to bone deposition, are also involved in the recruitment of osteoclasts and, therefore, regulate bone resorption (80).

Overall, we propose that branchpoint positioning could serve as a simple and straightforward model to study the (im)balance between bone resorption/antistitching and bone mineralization/prostitching activities. Ultimately, this system will provide a unique platform to study different compounds, signaling pathways, and molecular mechanisms toward the identification of new targets and the development of new therapeutic strategies.

Materials and Methods

Wild-type and transgenic zebrafish used in this study were from the AB strain. The lines used in this study were: *Tg(Ola.bglap:EGFP)^{hu4008}* (24), abbreviated *bglap:GFP*; *Tg(sp7:mCherry-Eco.NfsB)^{pd46}* (25), abbreviated *sp7:mCherry-NTR*; *Tg(Ola.ctsk:FRT-DsRed-FRT-Cre,myl7:EGFP)^{mh201}* (26), abbreviated *ctsk:DsRed*; *Tg(mpeg1.1:NTR-EYFP)^{w202}* (22), abbreviated *mpeg1.1:YFP*; *Tg(fli1:EGFP)^{y1}* (81), abbreviated *fli1:GFP*; *Tg(-5.2lyve1b:EGFP)^{nz150}* (67), abbreviated *lyve1b:GFP*; *Tg(-2.4shha-ABC:GFP)^{sb15}* (82), abbreviated *shha:GFP*.

Regeneration studies took place following amputation of the caudal fin 1–2 segments below the branchpoint of the most peripheral branching rays. The relative branchpoint position during the regenerative process was assessed by measuring the length from the amputation plane to the branchpoint divided by the total ray length from the amputation plane. Ablation studies were performed using metronidazole, as previously described (25). All other drug exposures were performed by immersion or intraperitoneal injections. Bone staining was performed as described, using alizarin red (70) or calcein (83). TRAP activity staining was performed as described (35). A complete description of the materials and methods can be found in the *SI Appendix, Materials and Methods*.

Data, Materials, and Software Availability. The RNA-seq dataset reported in this work has been deposited in the National Center for Biotechnology Information (NCBI) Gene Expression Omnibus (GEO), under accession number GSE205599 (https://www.ncbi.nlm.nih.gov/geo/query/acc.cgi?acc=GSE205599). All other study data are included in the article and/or *SI Appendix*.

ACKNOWLEDGMENTS. This study was funded by the Portuguese Foundation for Science and Technology (FCT) through the project UIDB/04326/2020 (to the CCMAR) and grant PD/BD/52425/2013 (to J.C.-d.-S.). Research in the Stainier lab is funded in part by the Max Planck Society. We thank Matthew Harris and Joana Caetano-Lopes for kindly providing the *ctsk:DsRed* transgenic line. We thank Srinath Ramkumar for his assistance in image acquisition.

Author affiliations: [a]Department of Developmental Genetics, Max Planck Institute for Heart and Lung Research, 61231 Bad Nauheim, Germany; [b]DZHK-German Centre for Cardiovascular Research, Partner Site Rhine-Main, 61231 Bad Nauheim, Germany; [c]CCMAR-Centre of Marine Sciences, University of Algarve, 8005-139 Faro, Portugal; [d]INSERM-National Institute of Health and Medical Research, Atip-Avenir, Aix Marseille University, Marseille Medical Genetics, 13005 Marseille, France; [e]CEDOC-Chronic Diseases Research Center, NOVA Medical School, NOVA University of Lisbon, 1150-082 Lisbon, Portugal; [f]STAB VIDA-Investigação e Serviços em Ciências Biológicas, 2825-182 Caparica, Portugal; and [g]FMCB-Faculty of Medicine and Biomedical Sciences and ABC-Algarve Biomedical Center, University of Algarve, 8005-139 Faro, Portugal

1. A. Salhotra, H. N. Shah, B. Levi, M. T. Longaker, Mechanisms of bone development and repair. *Nat. Rev. Mol. Cell Biol.* **21**, 696–711 (2020).
2. J.-M. Kim, C. Lin, Z. Stavre, M. B. Greenblatt, J.-H. Shim, Osteoblast-osteoclast communication and bone homeostasis. *Cells* **9**, 1–14 (2020).
3. W. A. Fernando *et al.*, Wound healing and blastema formation in regenerating digit tips of adult mice. *Dev. Biol.* **350**, 301–310 (2011).
4. M. Gemberling, T. J. Bailey, D. R. Hyde, K. D. Poss, The zebrafish as a model for complex tissue regeneration. *Trends Genet.* **29**, 611–620 (2013).
5. M.-A. Akimenko, M. Marí-Beffa, J. Becerra, J. Géraudie, Old questions, new tools, and some answers to the mystery of fin regeneration. *Dev. Dyn.* **226**, 190–201 (2003).
6. C. Pfefferli, A. Jaźwińska, The art of fin regeneration in zebrafish. *Regeneration* **2**, 72–83 (2015).
7. I. M. Sehring, G. Weidinger, Recent advancements in understanding fin regeneration in zebrafish. *Dev. Biol.* **9**, 1–16 (2020).
8. S. Stewart, K. Stankunas, Limited dedifferentiation provides replacement tissue during zebrafish fin regeneration. *Dev. Biol.* **365**, 339–349 (2012).
9. J. Becerra, G. S. Montes, S. R. Bexiga, L. C. Junqueira, Structure of the tail fin in teleosts. *Cell Tissue Res.* **230**, 127–137 (1983).
10. M. Marí-Beffa, J. A. Santamaría, P. Fernández-Llebrez, J. Becerra, Histochemically defined cell states during tail fin regeneration in teleost fishes. *Differentiation* **60**, 139–149 (1996).
11. G. S. Montes, J. Becerra, O. Toledo, M. Gordilho, L. Junqueira, Fine structure and histochemistry of the tail fin ray in teleosts. *Histochemistry* **75**, 363–376 (1982).
12. J. Cardeira *et al.*, Quantitative assessment of the regenerative and mineralogenic performances of the zebrafish caudal fin. *Sci. Rep.* **6**, 39191 (2016).
13. H. Nakagawa, J. Kuroda, T. Aramaki, S. Kondo, Mechanical role of actinotrichia in shaping the caudal fin of zebrafish. *Dev. Biol.* **481**, 52–63 (2022).
14. C. Murciano *et al.*, Ray and inter-ray blastemas interact to control bifurcations of *Danio rerio* fin rays. *Int. J. Dev. Biol.* **45**, S129–S130 (2001).
15. C. Murciano *et al.*, Ray-interray interactions during fin regeneration of *Danio rerio*. *Dev. Biol.* **224**, 214–224 (2002).
16. J. Capdevila, J. C. I. Belmonte, Patterning mechanisms controlling vertebrate limb development. *Annu. Rev. Cell Dev. Biol.* **17**, 87–132 (2001).
17. R. D. Riddle, R. L. Johnson, E. Laufer, C. Tabin, *Sonic hedgehog* mediates the polarizing activity of the ZPA. *Cell* **75**, 1401–1416 (1993).
18. L. Laforest *et al.*, Involvement of the *Sonic hedgehog*, *patched 1* and *bmp2* genes in patterning of the zebrafish dermal fin rays. *Development* **125**, 4175–4184 (1998).
19. B. E. Armstrong, A. Henner, S. Stewart, K. Stankunas, Shh promotes direct interactions between epidermal cells and osteoblast progenitors to shape regenerated zebrafish bone. *Development* **144**, 1165–1176 (2017).
20. J. A. Braunstein, A. E. Robbins, S. Stewart, K. Stankunas, asal epidermis collective migration and local Sonic hedgehog signaling promote skeletal branching morphogenesis in zebrafish fins. *Dev. Biol.* **477**, 177–190 (2021).
21. A. S. Azevedo, S. Sousa, A. Jacinto, L. Saúde, An amputation resets positional information to a proximal identity in the regenerating zebrafish caudal fin. *BMC Dev. Biol.* **12**, 24 (2012).
22. T. A. Petrie *et al.*, Macrophages modulate adult zebrafish tail fin regeneration. *Development* **141**, 2581–2591 (2014).
23. P. Dagenais *et al.*, Hydrodynamic stress and phenotypic plasticity of the zebrafish regenerating fin. *J. Exp. Biol.* **224**, jeb242309 (2021).

24. F. Knopf *et al.*, Bone regenerates via dedifferentiation of osteoblasts in the zebrafish fin. *Dev. Cell* **20**, 713–724 (2011).
25. S. P. Singh, J. E. Holdway, K. D. Poss, Regeneration of amputated zebrafish fin rays from de novo osteoblasts. *Dev. Cell* **22**, 879–886 (2012).
26. J. Caetano-Lopes *et al.*, Unique and non-redundant function of *csf1r* paralogues in regulation and evolution of post-embryonic development of the zebrafish. *Development* **147**, dev181834 (2020).
27. P. E. Witten, W. Villwock, Growth requires bone resorption at particular skeletal elements in a teleost fish with acellular bone (*Oreochromis niloticus*, Teleostei: Cichlidae). *J. Appl. Ichthyol.* **13**, 149–158 (1997).
28. C. H. Chesnut *et al.*, Salmon calcitonin: A review of current and future therapeutic indications. *Osteoporos. Int.* **19**, 479–491 (2008).
29. D. Mukherjee, U. Sen, S. P. Bhattacharyya, D. Mukherjee, The effects of calcitonin on plasma calcium levels and bone metabolism in the fresh water teleost *Channa punctatus*. *Comp. Biochem. Physiol. A Mol. Integr. Physiol.* **138**, 417–426 (2004).
30. N. Suzuki, T. Suzuki, T. Kurokawa, Suppression of osteoclastic activities by calcitonin in the scales of goldfish (freshwater teleost) and nibbler fish (seawater teleost). *Peptides* **21**, 115–124 (2000).
31. R. S. Hardy, H. Zhou, M. J. Seibel, M. S. Cooper, Glucocorticoids and bone: Consequences of endogenous and exogenous excess and replacement therapy. *Endocr. Rev.* **39**, 519–548 (2018).
32. F. Bauss, D. W. Dempster, Effects of ibandronate on bone quality: Preclinical studies. *Bone* **40**, 265–273 (2007).
33. H. H. Conaway, P. Henning, U. H. Lerner, Vitamin a metabolism, action, and role in skeletal homeostasis. *Endocr. Rev.* **34**, 766–797 (2013).
34. N. Blum, G. Begemann, Osteoblast de- and redifferentiation is controlled by a dynamic response to retinoic acid during zebrafish fin regeneration. *Development* **142**, 2894–2903 (2015).
35. N. Blum, G. Begemann, Retinoic acid signaling spatially restricts osteoblasts and controls ray-interray organization during zebrafish fin regeneration. *Development* **142**, 2888–2893 (2015).
36. F. V. Mariani, G. R. Martin, Deciphering skeletal patterning: Clues from the limb. *Nature* **423**, 319–325 (2003).
37. T. Nakamura, A. R. Gehrke, J. Lemberg, J. Szymaszek, N. H. Shubin, Digits and fin rays share common developmental histories. *Nature* **537**, 225–228 (2016).
38. T. Yano, K. Tamura, The making of differences between fins and limbs. *J. Anat.* **222**, 100–113 (2013).
39. T. Yano, G. Abe, H. Yokoyama, K. Kawakami, K. Tamura, Mechanism of pectoral fin outgrowth in zebrafish development. *Development* **139**, 2916–2925 (2012).
40. M. A. Akimenko, M. Ekker, Anterior duplication of the *Sonic hedgehog* expression pattern in the pectoral fin buds of zebrafish treated with retinoic acid. *Dev. Biol.* **170**, 243–247 (1995).
41. C. J. Watson, R. Y. Kwon, Osteogenic programs during zebrafish fin regeneration. *Bonekey Rep.* **4**, 745 (2015).
42. A. S. Brandão *et al.*, Yap induces osteoblast differentiation by modulating Bmp signalling during zebrafish caudal fin regeneration. *J. Cell Sci.* **132**, jcs231993 (2019).
43. K. Ando, E. Shibata, S. Hans, M. Brand, A. Kawakami, Osteoblast production by reserved progenitor cells in zebrafish bone regeneration and maintenance. *Dev. Cell* **43**, 643–650.e3 (2017).
44. S. Sousa *et al.*, Differentiated skeletal cells contribute to blastema formation during zebrafish fin regeneration. *Development* **138**, 3897–3905 (2011).
45. E. Quint *et al.*, Bone patterning is altered in the regenerating zebrafish caudal fin after ectopic expression of *sonic hedgehog* and *bmp2b* or exposure to cyclopamine. *Proc. Natl. Acad. Sci. U.S.A.* **99**, 8713–8718 (2002).
46. J. Zhang, S. Jeradi, U. Strähle, M.-A. Akimenko, Laser ablation of the sonic hedgehog-a-expressing cells during fin regeneration affects ray branching morphogenesis. *Dev. Biol.* **365**, 424–433 (2012).
47. T. Negishi-Koga *et al.*, Suppression of bone formation by osteoclastic expression of semaphorin 4D. *Nat. Med.* **17**, 1473–1480 (2011).
48. E. H. Burger, In vitro formation of osteoclasts from long-term cultures of bone marrow mononuclear phagocytes. *J. Exp. Med.* **156**, 1604–1614 (1982).
49. D. G. Walker, Control of bone resorption by hematopoietic tissue. The induction and reversal of congenital osteopetrosis in mice through the use of bone marrow and splenic transplants. *J. Exp. Med.* **142**, 651–663 (1975).
50. K. Henriksen, J. Bollerslev, V. Everts, M. A. Karsdal, Osteoclast activity and subtypes as a function of physiology and pathology - Implications for future treatments of osteoporosis. *Endocr. Rev.* **32**, 31–63 (2011).
51. S. L. Teitelbaum, Bone resorption by osteoclasts. *Science* **289**, 1504–1508 (2000).
52. S. L. Teitelbaum, Osteoclasts: What do they do and how do they do it? *Am. J. Pathol.* **170**, 427–35 (2007).
53. H. K. Väänänen, H. Zhao, "Osteoclast function: Biology and mechanisms" in *Principles of Bone Biology*, J. P. Bilezikian, L. G. Raisz, T. J. Martin, Eds. (Academic Press, 2008), pp. 193–209.
54. D. Brömme, K. Okamoto, B. B. Wang, S. Biroc, Human cathepsin O2, a matrix protein-degrading cysteine protease expressed in osteoclasts. Functional expression of human cathepsin O2 in Spodoptera frugiperda and characterization of the enzyme. *J. Biol. Chem.* **271**, 2126–2132 (1996).
55. T. Inaoka *et al.*, Molecular cloning of human cDNA for cathepsin K: Novel cysteine proteinase predominantly expressed in bone. *Biochem. Biophys. Res. Commun.* **206**, 89–96 (1995).
56. T. Inui *et al.*, Cathepsin K antisense oligodeoxynucleotide inhibits osteoclastic bone resorption. *J. Biol. Chem.* **272**, 8109–8112 (1997).
57. P. Saftig *et al.*, Impaired osteoclastic bone resorption leads to osteopetrosis in cathepsin-K-deficient mice. *Proc. Natl. Acad. Sci. U.S.A.* **95**, 13453–13458 (1998).
58. K. Kusano *et al.*, Regulation of matrix metalloproteinases (MMP-2, -3, -9, and -13) by interleukin-1 and interleukin-6 in mouse calvaria: Association of MMP induction with bone resorption. *Endocrinology* **139**, 1338–1345 (1998).
59. C. Minkin, Bone acid phosphatase: Tartrate-resistant acid phosphatase as a marker of osteoclast function. *Calcif. Tissue Int.* **34**, 285–290 (1982).
60. C. P. Price, A. Kirwan, C. Vader, Tartrate-resistant acid phosphatase as a marker of bone resorption. *Clin. Chem.* **41**, 641–643 (1995).
61. M. B. Madel *et al.*, Immune function and diversity of osteoclasts in normal and pathological conditions. *Front. Immunol.* **10**, 1408 (2019).
62. S. G. Romeo *et al.*, Endothelial proteolytic activity and interaction with non-resorbing osteoclasts mediate bone elongation. *Nat. Cell Biol.* **21**, 430–441 (2019).
63. M. Monroy, A. L. McCarter, D. Hominick, N. Cassidy, M. T. Dellinger, Lymphatics in bone arise from pre-existing lymphatics. *Development* **147**, dev184291 (2020).
64. Q. Zhang *et al.*, VEGF-C, a lymphatic growth factor, is a RANKL target gene in osteoclasts that enhances osteoclastic bone resorption through an autocrine mechanism. *J. Biol. Chem.* **283**, 13491–13499 (2008).
65. K. Takeyama, M. Chatani, Y. Takano, A. Kudo, In-vivo imaging of the fracture healing in medaka revealed two types of osteoclasts before and after the callus formation by osteoblasts. *Dev. Biol.* **394**, 292–304 (2014).
66. D. Castranova *et al.*, Live imaging of intracranial lymphatics in the zebrafish. *Circ. Res.* **128**, 42–58 (2021).
67. K. S. Okuda *et al.*, *lyve1* expression reveals novel lymphatic vessels and new mechanisms for lymphatic vessel development in zebrafish. *Development* **139**, 2381–2391 (2012).
68. H. Y. Lim *et al.*, Hyaluronan receptor LYVE-1-expressing macrophages maintain arterial tone through hyaluronan-mediated regulation of smooth muscle cell collagen. *Immunity* **49**, 326–341 (2018).
69. D. Gancz *et al.*, Distinct origins and molecular mechanisms contribute to lymphatic formation during cardiac growth and regeneration. *Elife* **8**, e44153 (2019).
70. A. Bensimon-Brito *et al.*, Revisiting in vivo staining with alizarin red S - a valuable approach to analyse zebrafish skeletal mineralization during development and regeneration. *BMC Dev. Biol.* **16**, 2 (2016).
71. V. Laizé, P. J. Gavaia, M. L. Cancela, Fish: A suitable system to model human bone disorders and discover drugs with osteogenic or osteotoxic activities. *Drug Discov. Today Dis. Model.* **13**, 29–37 (2014).
72. D. Oppedal, M. I. Goldsmith, A chemical screen to identify novel inhibitors of fin regeneration in zebrafish. *Zebrafish* **7**, 53–60 (2010).
73. A. M. Recidoro *et al.*, Botulinum toxin induces muscle paralysis and inhibits bone regeneration in zebrafish. *J. Bone Miner. Res.* **29**, 2346–2356 (2014).
74. H. Bi *et al.*, Key triggers of osteoclast-related diseases and available strategies for targeted therapies: A review. *Front. Med.* **4**, 234 (2017).
75. J. A. White, M. B. Boffa, B. Jones, M. Petkovich, A zebrafish retinoic acid receptor expressed in the regenerating caudal fin. *Development* **120**, 1861–1872 (1994).
76. T. J. Cunningham, G. Duester, Mechanisms of retinoic acid signalling and its roles in organ and limb development. *Nat. Rev. Mol. Cell Biol.* **16**, 110–123 (2015).
77. S. Kujawski *et al.*, Calcineurin regulates coordinated outgrowth of zebrafish regenerating fins. *Dev. Cell* **28**, 573–587 (2014).
78. L. Sun *et al.*, Evidence that calcineurin is required for the genesis of bone-resorbing osteoclasts. *Am. J. Physiol. Ren. Physiol.* **292**, F285–F291 (2007).
79. M. Tarasco *et al.*, New insights into benzo[α]pyrene osteotoxicity in zebrafish. *Ecotoxicol. Environ. Saf.* **226**, 112838 (2021).
80. Z. Xiao, L. D. Quarles, Physiological mechanisms and therapeutic potential of bone mechanosensing. *Rev. Endocr. Metab. Disord.* **16**, 115–129 (2015).
81. N. D. Lawson, B. M. Weinstein, imaging of embryonic vascular development using transgenic zebrafish. *Dev. Biol.* **248**, 307–318 (2002).
82. A. Shkumatava, S. Fischer, F. Müller, U. Strahle, C. J. Neumann, Sonic hedgehog, secreted by amacrine cells, acts as a short-range signal to direct differentiation and lamination in the zebrafish retina. *Development* **131**, 3849–3858 (2004).
83. S. J. Du, V. Frenkel, G. Kindschi, Y. Zohar, Visualizing normal and defective bone development in zebrafish embryos using the fluorescent chromophore calcein. *Dev. Biol.* **238**, 239–246 (2001).